RESEARCH ARTICLE
SPACE PHYSICS: MAGNETOSPHERIC PHYSICS

Earth and Planetary Physics
8: 222–233, 2024
doi: 10.26464/epp2023066

Magnetopause properties at the dusk magnetospheric flank from global magnetohydrodynamic simulations, the kinetic Vlasov equilibrium, and in situ observations — Potential implications for SMILE

Marius Echim[1,2,3*], Costel Munteanu[1], Gabriel Voitcu[1], and Eliza Teodorescu[1]

[1]Institute of Space Science, Măgurele 077125, Romania;

[2]Royal Belgian Institute for Space Aeronomy, 1180 Brussels, Belgium;

[3]Solar-Terrestrial Centre of Excellence (STCE), 1180 Brussels, Belgium

Key Points:

- Global three-dimensional time-dependent simulations of the Earth's magnetosphere were performed for interplanetary conditions corresponding to in situ observations of the dusk flank magnetopause (MP) by the Magnetospheric Multiscale 2 (MMS2) spacecraft.
- One-dimensional stationary Vlasov equilibrium solutions computed for asymptotic conditions derived from the same MMS2 observations were used to initialize the global magnetohydrodynamic (MHD) simulations.
- The results showed similarities and differences between global simulations, Vlasov modeling, and observations. A notable difference was that the MP thickness obtained from global MHD simulations was one order of magnitude larger than the MP scales observed by the MMS2; the kinetic model was in reasonable agreement.

Citation: Echim, M., Munteanu, C., Voitcu, G., and Teodorescu, E. (2024). Magnetopause properties at the dusk magnetospheric flank from global magnetohydrodynamic simulations, the kinetic Vlasov equilibrium, and in situ observations — Potential implications for SMILE. *Earth Planet. Phys.*, *8*(1), 222–233. http://doi.org/10.26464/epp2023066

Abstract: We derived the properties of the terrestrial magnetopause (MP) from two modeling approaches, one global–fluid, the other local–kinetic, and compared the results with data collected in situ by the Magnetospheric Multiscale 2 (MMS2) spacecraft. We used global magnetohydrodynamic (MHD) simulations of the Earth's magnetosphere (publicly available from the NASA-CCMC [National Aeronautics and Space Administration–Community Coordinated Modeling Center]) and local Vlasov equilibrium models (based on kinetic models for tangential discontinuities) to extract spatial profiles of the plasma and field variables at the Earth's MP. The global MHD simulations used initial solar wind conditions extracted from the OMNI database at the time epoch when the MMS2 observes the MP. The kinetic Vlasov model used asymptotic boundary conditions derived from the same in situ MMS measurements upstream or downstream of the MP. The global MHD simulations provide a three-dimensional image of the magnetosphere at the time when the MMS2 crosses the MP. The Vlasov model provides a one-dimensional local view of the MP derived from first principles of kinetic theory. The MMS2 experimental data also serve as a reference for comparing and validating the numerical simulations and modeling. We found that the MP transition layer formed in global MHD simulations was generally localized closer to the Earth (roughly by one Earth radius) from the position of the real MP observed by the MMS. We also found that the global MHD simulations overestimated the thickness of the MP transition by one order of magnitude for three analyzed variables: magnetic field, density, and tangential speed. The MP thickness derived from the local Vlasov equilibrium was consistent with observations for all three of these variables. The overestimation of density in the Vlasov equilibrium was reduced compared with the global MHD solutions. We discuss our results in the context of future SMILE (Solar wind Magnetosphere Ionosphere Link Explorer) campaigns for observing the Earth's MP.

Keywords: magnetopause; magnetohydrodynamic numerical simulations; Vlasov equilibrium; Magnetospheric Multiscale observations

1. Introduction

The solar wind–magnetosphere–ionosphere system and the mutual interactions among its elements are key research topics for the Solar wind Magnetosphere Ionosphere Link Explorer (SMILE) mission (Raab et al., 2016; Branduardi-Raymont and Wang C, 2022). Because of its innovative observational strategy, SMILE will allow for unprecedented global views of the dynamics of the magnetosphere in response to solar wind variability. In preparation for the operational phase, various magnetospheric configurations are being examined and simulated numerically to anticipate the key observational elements and evaluate the response of the

Correspondence to: M. Echim, echim@spacescience.ro
Received 01 JUL 2023; Accepted 11 SEP 2023.
First Published online 14 NOV 2023.

mission instruments, particularly the Soft X-ray Imager telescope, SMILE SXI (Soman et al., 2018), to various possible configurations of the solar wind–magnetosphere–ionosphere system.

Global magnetohydrodynamic (MHD) numerical simulations provide a global three-dimensional (3-D) view of the Earth's magnetosphere and of its time-dependent dynamic response to solar wind variable driving. Different variants of the global simulations apply different strategies to solve the MHD set of equations. The solutions provide tables of 3-D global or regional physical observables, which can be fed to numerical implementations of the SMILE instruments, particularly the SXI, and simulate how the instruments "see" the (virtual) reality pictured by global simulations. In this way, one can imagine the response of the instrument to various magnetospheric dynamic states and can imagine in advance different typologies and limitations (e.g., Samsonov et al., 2022a, b). One key goal is to better understand various types of signatures in the SXI data and how they reveal different magnetospheric configurations. One can then investigate their complexity as a function of the observational reality captured by numerical simulations.

In this work, we analyzed a set of numerical simulations and models built to reveal the properties of the magnetopause (MP), such as the transition of physical parameters between the asymptotic (upstream and downstream) states, the MP spatial scale or thickness, and how the MP properties change as a function of the local time. We also discuss the limitations introduced by global MHD simulations and Vlasov modeling compared with in situ measurements.

The MP is often called the outer boundary of the geomagnetic field cavity and is defined by the 3-D surface separating the terrestrial plasma and magnetic field from the plasma and field of interplanetary or solar origin. Predicted theoretically by Chapman and Ferraro (1930) as a surface electric current layer separating the Earth's magnetic field from the incoming solar wind (not yet discovered at that epoch), the MP was revealed by in situ measurements of the first spacecraft of the space era. Cahill and Amazeen (1963) published the first report on the magnetic properties of the MP from Explorer 12 data. Since then, a fleet of spacecraft have probed the MP for various local times and interplanetary conditions.

Magnetohydrodynamic discontinuities (Hudson, 1970) are theoretical building blocks defined as ideal plane surfaces where the field and plasma undergo sharp or infinitesimal jumps fulfilling MHD jump conditions extracted from classical electro- and hydrodynamic approaches derived from the conservation of mass, momentum, and energy (e.g., see Gurnett and Bhattacharjee, 2017). Tangential discontinuities are a subclass of MHD discontinuities in which the plasma flow is tangential to the interface and the magnetic field component normal to it is equal to zero. No cross transport occurs in a tangential discontinuity; the asymptotic plasmas are fully separated.

Vlasov modeling of sharp plasma interfaces was investigated in the 1960s and 1970s, particularly because of the interest this topic raised among the laboratory and fusion plasma communities (Sestero, 1964, 1966, 1967). Soon after, the theoretical insight was further developed in the context of interplanetary plasma interfaces and magnetic holes (Lemaire and Burlaga, 1976; Burlaga and Lemaire, 1978) and applied for investigating the structure of the terrestrial MP (Roth, 1978; Whipple et al., 1984; De Keyser and Roth, 1997, 1998; for a review, see Roth et al., 1996). The above-cited works provide one-dimensional (1-D) solutions, whereas a two-dimensional (2-D) description was given by Echim and Lemaire (2005).

A recent review by Haaland et al. (2021) summarizes 20 years of in situ MP observations by Cluster (Escoubet et al., 1997), a mission that contributes enormously to understanding the properties and dynamics of the MP. Among the findings emphasized by Haaland et al. (2021), we mention a consistent estimation of MP motion with velocities up to 80 km/s, an evaluation of MP thickness that is on the order of several hundred kilometers, and a spatial scaling corresponding to a few magnetosheath ion Larmor gyroradii.

2. Methods, Models, and Data

2.1 Global 3-D Time-Dependent MHD Simulations on the NASA-CCMC Models with an SWMF/GM (BATS-RUS) Approach

Part of the numerical simulation efforts devoted to SMILE are supported by global magnetospheric models available from the National Aeronautics and Space Administration–Community Coordinated Modeling Center (NASA-CCMC). One of the most popular codes is the University of Michigan's Multifluid Block-Adaptive-Tree Solar wind Roe-type Upwind Scheme (BATS-RUS), also known as the Global Magnetosphere module of the Space Weather Modeling Framework (SWMF/GM). The SWMF/GM module performs an ideal MHD numerical simulation of the global magnetosphere (Gombosi et al., 2002; Tóth et al., 2006, 2008; Glocer et al., 2009). The SWMF/GM (BATS-RUS) simulation package allows for different types of grids; the inner boundary considered by the SWMF/GM is a sphere of radius 2.5 R_E (Earth radii) centered on the Earth. The simulation domain expands from 32 R_E upstream to 224 R_E downstream of the planet (Glocer et al., 2009). The model spatial resolution varies from 0.06 R_E close to the Earth, 0.125 R_E close to the nose, and 8 R_E near the outer edges (in the solar wind). The model is available from the NASA–CCMC to run on request (https://ccmc.gsfc.nasa.gov/tools/runs-on-request/).

The model provides time-dependent values for plasma parameters, such as the density, N; the pressure, P; three components of the plasma bulk velocity (in the ideal MHD approach) V_x, V_y, V_z; three components of the magnetic field B_x, B_y, B_z; and three components of the electric current density, J_x, J_y, J_z. The results are available as global 3-D maps; various plotted 2-D sections are offered as options. The code also provides the possibility of simulating satellite trajectories to collect numerical simulation data as time series recorded by virtual satellites launched in the simulation domain.

2.2 One-Dimensional Stationary Vlasov Equilibrium Models

A kinetic Vlasov description of plasma interfaces is based on the

first principles of plasma kinetic theory (Tidman and Montgomery, 1964; Delcroix and Bers, 1994). The building blocks are provided by a solution to the Vlasov equation specifying $f_\alpha(\boldsymbol{r},\boldsymbol{v})$, the velocity distribution function of electrons and ions,

$$\frac{\partial f_\alpha}{\partial t}+\boldsymbol{v}\cdot\frac{\partial f_\alpha}{\partial \boldsymbol{r}}+\frac{q_\alpha}{m_\alpha}[\boldsymbol{E}+\boldsymbol{v}\times\boldsymbol{B}]\cdot\frac{\partial f_\alpha}{\partial \boldsymbol{v}}=0, \tag{1}$$

where $\frac{q_\alpha}{m_\alpha}[\boldsymbol{E}+\boldsymbol{v}\times\boldsymbol{B}]$ is the electromagnetic force acting on the charged particles, α. The Vlasov equation is coupled with Maxwell's equations, which provide the electric field, $\boldsymbol{E}$, and the magnetic field, $\boldsymbol{B}$, to be used in Equation (1). Note that in Vlasov equilibrium modeling, the charge and current densities considered to be the "sources" of the electromagnetic field in Maxwell's equations are derived as moments of the velocity distribution functions provided by the solutions to the Vlasov equation. For a discussion on the coupling between the Vlasov and Maxwell's equations, see Echim et al. (2011).

This system of equations is solved in the stationary case when the time dependence is disregarded. Another fundamental assumption is that the component of the magnetic field normal to the surface of the interface is equal to zero. Even under such a strict hypothesis, the degree of complexity of Vlasov equilibria is quite high, and such models can be applied for limited spatial regions, for instance in the vicinity of the MP. Therefore, although the kinetic solutions can reveal dynamic features or details at a high spatial and phase space resolution and can describe the dynamics of different species and populations, their spatial coverage is extremely limited compared with global–fluid models. Nevertheless, the usefulness of kinetic modeling for studies of the MP has been demonstrated and validated with in situ data (e.g., see Roth et al., 1996; De Keyser and Roth, 1997, 1998; Echim et al., 2011).

However, in the kinetic approach, the radical fluid assumptions are partially relaxed. Because, for a kinetic tangential discontinuity, there is no effective mass transport across, the tangential discontinuity is treated as a layer or sheath of finite thickness. The kinetic tangential discontinuity is the site of electric charge separation effects leading to an electric field normal to the interface; the internal structure of the kinetic tangential discontinuity is solved. That is, the model provides the profile of variation between the two asymptotic states of all parameters, plasma and field; thus, it can describe transitions with spatial scales as small as the electron Larmor radius.

In this study, we used kinetic Vlasov modeling to study the structure of the Earth's MP in a context adapted to SMILE mission scenarios. The 1-D tangential discontinuity is defined by two asymptotic plasma states and electromagnetic field states at the two sides, "left" and "right," of the discontinuity, for which the entire set of plasma and field parameters is specified as inputs for the numerical solution of the Vlasov–Maxwell set. Inside the transition layer, all the variables vary only along the boundary normal. The results discussed in this study were obtained for asymptotic states in which the plasma and field parameters were provided by in situ observations by the Magnetospheric Multiscale 2 (MMS2) spacecraft. Thus, the Vlasov model results could be compared with real crossings of the MP.

Starting from the two asymptotic states at the left and right of the transition, thus two point values, the Vlasov equilibrium self-consistently calculates the profile of transition between the two states by solving the Vlasov equation, the Poisson equation, and the Maxwell–Ampere equation. In the current implementation, the electrostatic potential was derived from the equation of quasi-neutrality instead of the Poisson equation. The plasma moments are known as analytical functions of the electric potential and magnetic vector potential, which in turn are provided by the quasineutrality equation and the Maxwell–Ampere equation. To achieve a solution that resembled the observations, we iterated over the asymptotic values of plasma variables, beginning from the values observed by MMS2, until the system reached convergence.

2.3 MMS2 Observations of the Earth's Magnetopause

An international team supported by the International Space Science Institute in Bern, Switzerland, has compiled a database of ~17,000 MP crossings by using MMS plasma and magnetic field data (Paschmann et al., 2018; Haaland et al., 2020). One of the important findings of this study is an evaluation of the MP thickness over the entire ensemble of data, indicating that the MP thickness changes from roughly 930 km in the dusk sector to roughly 735 km in the front (08–16 MLT [magnetic local time]) and roughly 860 km in the dawn. A previous investigation (Haaland and Gjerloev, 2013), based on Cluster data, indicated slightly larger values. We selected several MP crossings from this database in the three main magnetospheric regions, frontside, dusk, and dawn, for further study. The goal was to perform global simulations of the magnetosphere for the time periods when MMS2 crossed the MP and then compare the profiles provided by the simulations with the one measured in situ by MMS2. Paschmann et al. (2018) included in the database additional analyses of MMS data, for instance, the minimum variance analysis of magnetic field data (MVAB), and they used such analytical results for further processing of the data. Figure 1 shows an example of such a crossing at the dusk flank. The data recorded by MMS2 during this crossing were used in our study to perform tailored global MHD simulations and compute the Vlasov equilibrium solution for the MP, as explained next.

From the OMNI database, we extracted the solar wind parameters corresponding to the particular time of MP crossing by MMS2, as illustrated in Figure 1. In this way, we initialized the global magnetospheric simulation on the NASA-CCMC model with the SWMF/GM package, aiming to construct the global magnetospheric state for the conditions observed by MMS2. Thus, we simulated one hour of magnetospheric dynamics for a time interval beginning at 09:45:00 universal time (UT) and ending at 10:45:00 UT on October 16, 2015. The MMS2 spacecraft crossed the MP at 10:26:00 UT. These numerical simulations revealed the global 3-D time-dependent dynamics of the entire magnetosphere, as described by the ideal MHD equations solved by the SWMF/GM.

The plasma and field parameters measured by MMS2 upstream and downstream of the MP were also considered as inputs or asymptotic conditions for computing Vlasov equilibrium solutions for the MP. These models revealed the self-consistent, 1-D,

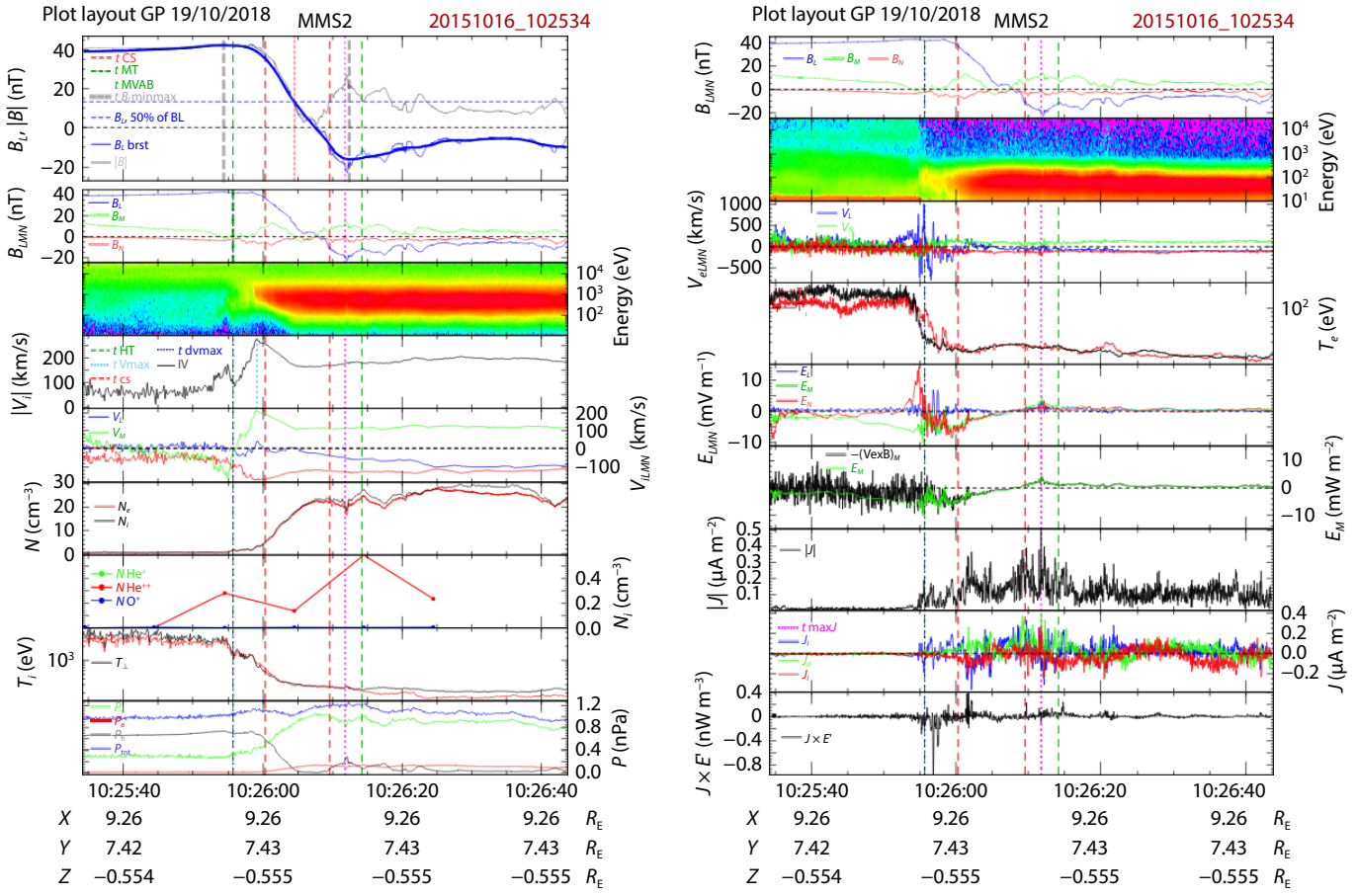

Figure 1. Example of a summary plot from the MMS database (Haaland et al., 2020) showing data from the MMS2 spacecraft during a MP outbound traversal on October 16, 2015. The data are shown in the GSE (Geocentric Solar Ecliptic) system.

stationary profile of the MP derived from first principles and the Vlasov–Maxwell equations, as discussed in the next section, together with a comparison with global MHD results.

The minimum variance analysis applied on magnetic field data (MVAB; e.g., see Sonnerup and Scheible, 1998) is the method used the most frequently to obtain the orientation of a discontinuity, based on the 1-D model of a current sheet. It is also the method widely applied to find the geometry and orientation of the MP from in situ measurements. Mathematically, this is achieved by constructing a magnetic covariance matrix and thereafter finding the eigenvectors and eigenvalues of this matrix. In the present work, we used a covariance matrix of the form discussed by Mailyan et al. (2008). In studies of the Earth's MP, the MVAB allows for the definition of a coordinate system, *LMN*, naturally aligned with the symmetry axis of the MP (e.g., see Munteanu et al., 2013; Paschmann et al., 2018).

The *LMN* coordinate system is local and has to be constructed for each MP crossing, using magnetic field measurements over a time interval on the order of a few minutes. The eigenvectors resulting from the MVAB form a rotation matrix with three orthogonal unit vectors: *L* (orientation of maximum variance), *M* (orientation of intermediate variance), and *N* (orientation of minimum variance). The *L* axis will typically be well defined for MP crossings because the maximum variance direction is largely governed by the magnetic field inside the magnetosphere. The *N* axis is typically perpendicular to the MP current sheet. We enforced an outward-pointing *N* direction. The *M* axis completes the right-handed system. The *LMN* reference was used in this study to represent data along virtual satellite trajectories injected in the 3-D magnetosphere simulated numerically with the SWMF. The reference system used to compute the Vlasov equilibrium solutions is consistent with *LMN* because all the Vlasov solution variables are specified as a function of the coordinate normal to the plasma interface.

3. Magnetopause Profiles from Global MHD Simulations Tailored to MMS2 Observations

The OMNI solar wind data recorded at the moment when MMS2 intersects the MP were used to initialize the global MHD simulations with the SWMF/GM code provided by the NASA-CCMC. In Figure 2a, we show a 2-D map of the plasma density in the dusk flank of the simulated magnetosphere captured at 10:26:00 UT, precisely the moment when MMS2 crossed the MP. The figure shows the magnetosheath, the MP, and the adjacent magnetospheric layers at the dusk flank, as well as the position of the MMS2 spacecraft.

The magnetic field data "recorded" along the true MMS2 orbit injected in the globally simulated magnetosphere showed no signature of a transition typical for the MP. Indeed, at 10:26 UT, the time when the MMS2 spacecraft intersected in situ the real MP,

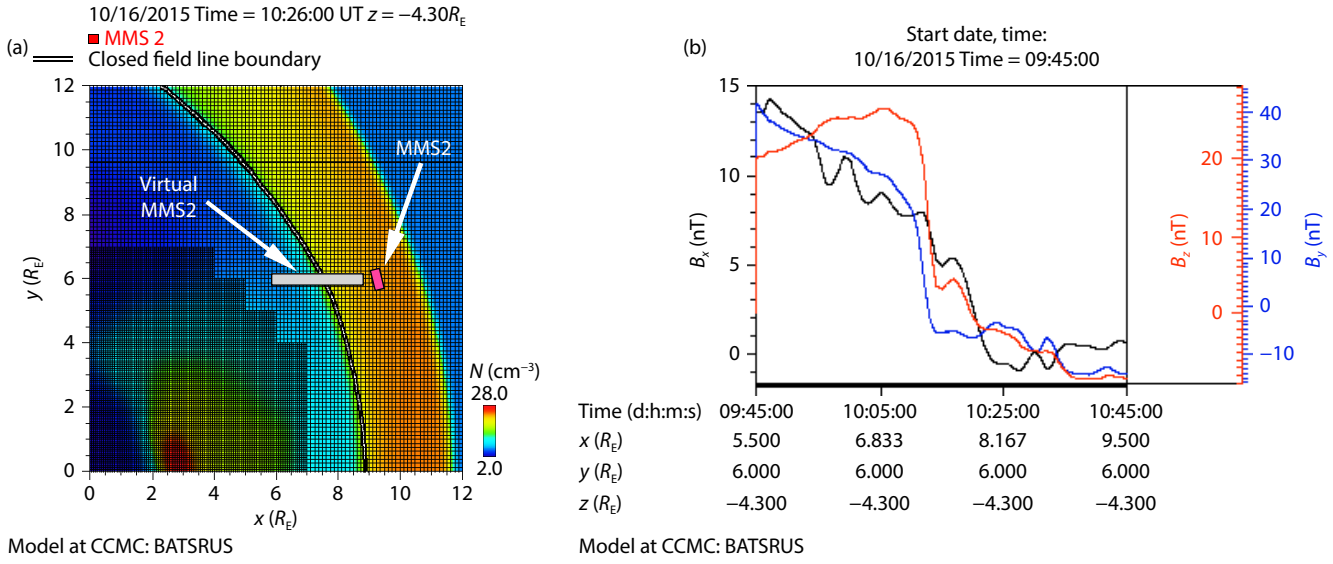

Figure 2. (a) A 2-D cross-section (for $Z_{GSE} = -4.3\ R_E$) through the 3-D map of plasma density produced by global simulations initialized with OMNI solar wind data corresponding to the MMS2 observations shown in Figure 1. (b) Magnetic field data from 3-D global MHD numerical simulations at the MP, in the dusk sector close to the MMS2 position.

the virtual spacecraft was localized far from the MP in the magnetosheath of the 3-D numerically simulated magnetosphere. The simulated MP was closer to the Earth by roughly 1.8 R_E compared with the position detected by in situ measurements of MMS2.

Nevertheless, we selected a crossing in the direction normal to the simulated MP; its profile is illustrated in Figure 2. The simulated magnetic field showed a transition with properties similar to the observed MP field but expanded over much larger scales. A note is in order here. The MP profile can be extracted from the global MHD simulations performed on the NASA-CCMC model in two ways:

(1) Take a time snapshot of the global 3-D numerically simulated magnetosphere and extract a 1-D spatial profile in the direction normal to the MP. This type of profile is further called sig1.
(2) Allow a virtual spacecraft to move along the virtual orbit, and at each time step, consider the magnetospheric state at that respective time, thus resulting a time-dependent sampling of the MP. This type is further called sig2.

To allow for a comparison between the numerical simulation results and in situ observations, we applied the MVAB analysis on the simulations (sig1 and sig2 data) and experimental results (from MMS2 on October 16, 2015) and transformed all the numerical and experimental data in the respective *LMN* frames, as shown in Figure 3. Note also that the MMS2 data are plotted as a function of the distance normal to the MP by considering the MP at a standstill.

However, in reality the MP generally has a relative speed with respect to the *LMN* reference frame. Khrabrov and Sonnerup (1998) proposed a method to estimate this relative velocity, which was tested on our data. As a preliminary estimation for the speed of the MP, we used a time analysis of the motion of the MP nose from OMNI data (shown in Figure 4). At approximately 10:26 UT, when the MP was intersected by MMS2, the OMNI data suggest an MP speed in the direction normal to the interface on the order of 10 km/s and less. Generally, the MP speed can take values up to 50–60 km/s (Haaland et al., 2021). The thickness of the MP, D_{MP}, can then be estimated from $D_{MP} = V_{MP} \times DT_{MP}$, where DT_{MP} is the duration that MMS2 intersects the MP layer.

We also checked the dynamics of the MP at the dusk side of the simulated magnetosphere, and we found a time variation of the MP consistent with what was found from the OMNI data. This time variation was confirmation that the global numerical simulations mimicked, at the magnetospheric dawn and dusk flanks, the MP dynamics observed experimentally at the frontside. In the following section, we consider an MP speed equal to 30 km/s.

4. Magnetopause Properties at the Dusk Magnetospheric Flank: A Comparison Between Global MHD Simulations, Vlasov Modeling, and MMS2 Data

In this section, we discuss the properties of the MP derived from global numerical simulations of the Earth's magnetosphere and from local kinetic Vlasov solutions, and then compare the numerical results with MMS2 in situ observations. The experimental data also served to initialize global simulations performed with SWMF/GM BATS-RUS models run on the NASA-CCMC. The asymptotic conditions for the Vlasov model were defined from a projection of MMS2 data in the *LMN* frame. This reference frame provides the natural reference for evaluating the transition profiles and is compatible with the 1-D kinetic Vlasov equilibrium, whose spatial coordinate is aligned with the direction normal to the interface. In Table 1, we specify the asymptotic conditions assumed for the Vlasov model, derived from MMS2 observations.

We focused our analysis on the transition profiles at the MP obtained for three variables: the magnetic field, the density, and the plasma tangential velocity. For each parameter, we traced on the same plot the profiles obtained from global MHD simulations,

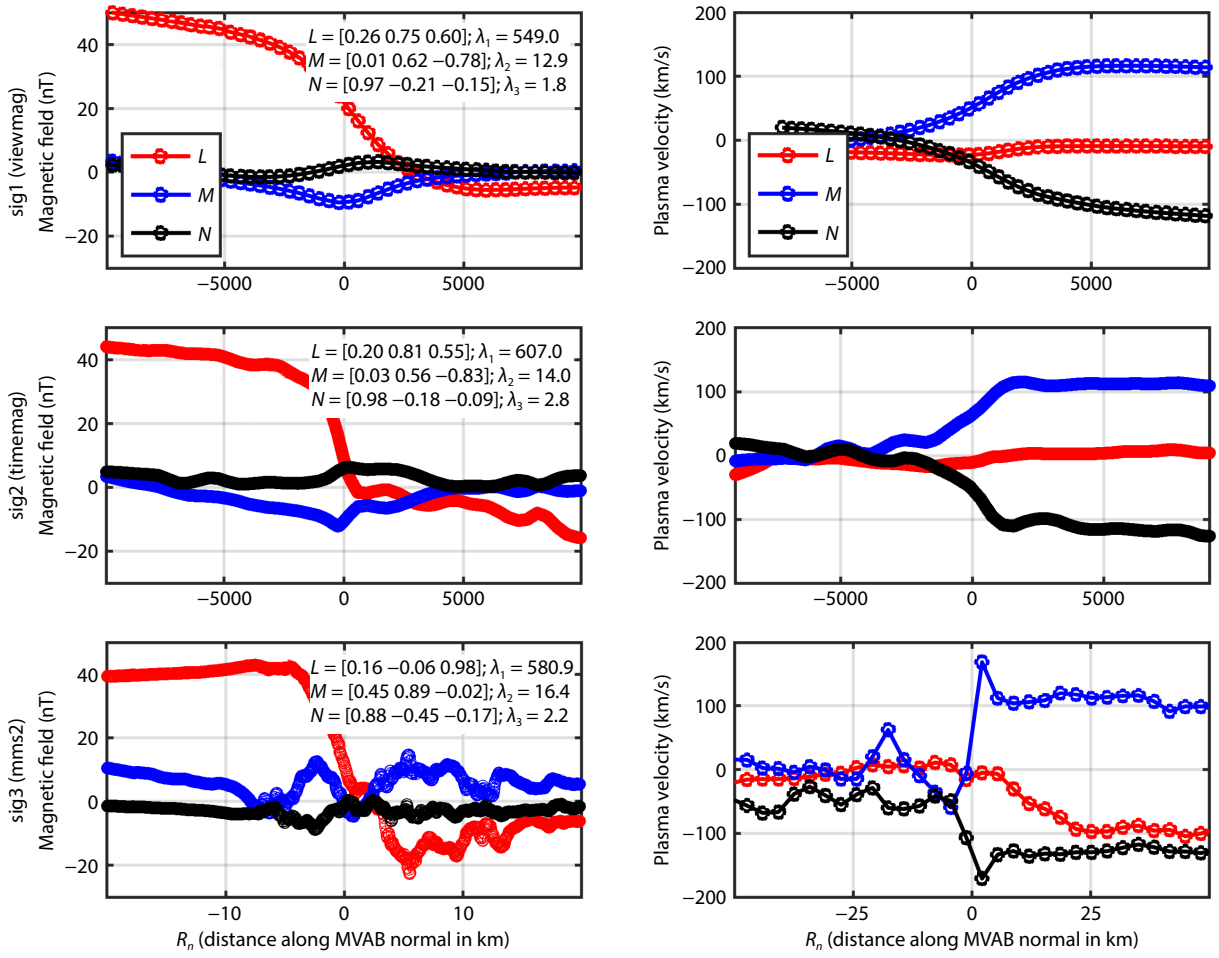

Figure 3. (left column) Magnetic field time series from global MHD simulations extracted from the virtual MMS2 intersecting the simulated MP (sig1 and sig2, see text) and real MMS2 observations (sig3) projected on the *LMN* reference frame aligned with the eigenvectors provided by the MVAB analysis. Note that the direction corresponding to the smallest eigenvalue is the direction normal to the MP surface. In addition, the data are plotted as a function of the coordinate R_n normal to the MP (specified in kilometers and centered on the MP location). In each panel, we also indicate the eigenvalues and eigenvectors provided by the MVAB. (right column) The plasma bulk velocity time series from simulations (sig1 and sig2) and MMS observations (sig3) projected on the *LMN* reference frame aligned with the eigenvectors retrieved from the MVAB analysis.

1-D Vlasov modeling, and in situ measurements by MMS2.

Figure 5 shows the magnetic field transition profile as a function of the coordinate normal to the MP and over a spatial range on the order of 20,000 km. Figure 6 shows an enlarged view over the central region of this transition, expanding more than 2000 km. The four profiles were displaced along the R_n axis such that the center of the transition (the maximum gradient) would fall in R_n = 0 for all signals. The same displacement was applied for all subsequent figures. Note, however, that the displacement was different for the different variables (magnetic field, density, velocity) because the center of transition was localized in different positions for the different parameters.

The MP magnetic field transition provided by the global MHD simulations had a spatial scale on the order of Λ_{MHD} = 8000 km. The total magnetic jump, between upstream and downstream MP asymptotic values, was on the order of 40 nT.

The signal extracted from the time-dependent simulation (sig2) was projected in the direction normal to the MP, assuming an MP speed on the order of 30 km/s. The same MP speed was considered when the MMS2 data were projected in the normal direction.

Figure 6 shows that the spatial scale of the kinetic model derived for asymptotic parameters prescribed from MMS2 data was on the order of 800 km, very close to the spatial scale observed in situ by MMS2. However, the magnetic field from the Vlasov model shows an overall offset equal to 20 nT. (This offset is compensated for in Figure 6.) The magnetic jump provided by the Vlasov model was equal to 60 nT, in close agreement with MMS2 observations.

The global MHD simulations performed with the SWMF/GM provide a proxy for the location of the MP as the boundary between open and closed geomagnetic field lines. This transition takes place by definition on a 3-D infinitesimal surface; no scale is associated with it. However, in reality, there is uncertainty regarding the location of this surface, which is given by the spatial resolution of the numerical simulations, equal to 0.125 R_E in our case. Note also that the open–closed boundary is located in R_n = 510 km in Figure 6. However, this MP position is relevant only for

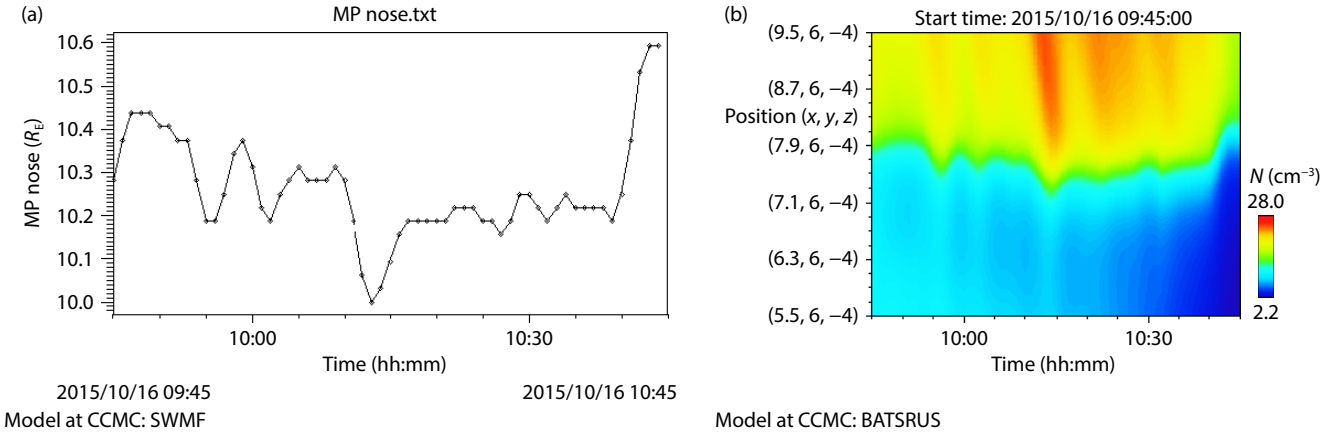

Figure 4. (a) Estimation of the time dependence of the MP nose position from OMNI data. (b) Estimation of the *X* GSE coordinate of the MP position at the dusk flank, in *Y* GSE = 6 R_E, *Z* GSE = −4 R_E, from global magnetospheric conditions tailored for MMS2 observations; the panel shows the plasma density.

Table 1. Asymptotic conditions downstream/left (side 1) and upstream/right (side 2) of the Vlasov equilibrium model.[a]

N_{eo1} (cm^{-3})	N_{io1} (cm^{-3})	T_{eo1} (eV)	T_{io1} (eV)	V_{eo1} (km/s)	V_{io1} (km/s)
0.01	0.01	1000	1000	0; 0	0; 0
N_{eo2} (cm^{-3})	N_{io2} (cm^{-3})	T_{eo2} (eV)	T_{io2} (eV)	V_{eo2} (km/s)	V_{io2} (km/s)
5	5	200	200	0; −95	0; −95

[a]"N_{eo}/N_{io}" indicates the density of "outer" electrons/ions (in cm^{-3}). "T_{eo}/T_{io}" and "V_{eo}/V_{io}" indicate temperature (in eV) and average velocity (the two components tangential to the interface, in km/s) for the same outer populations, electrons/ions.

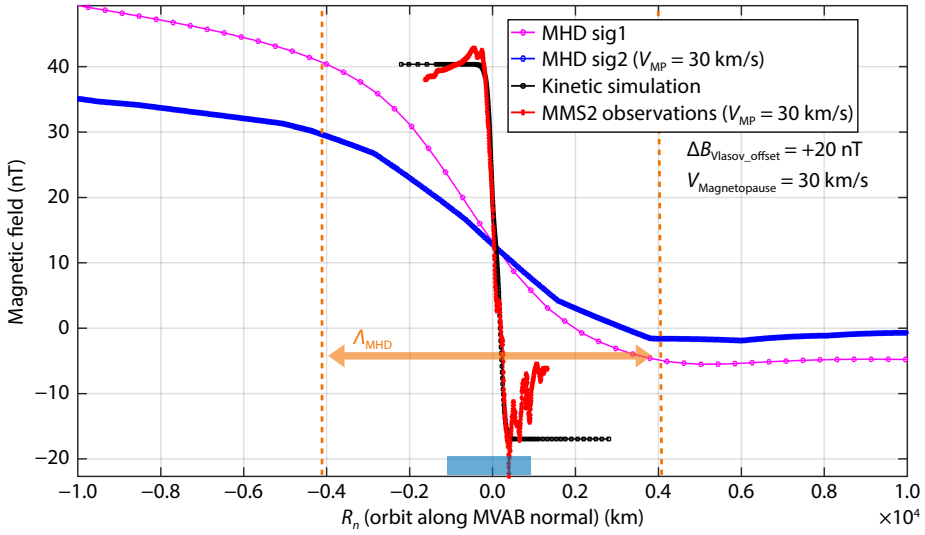

Figure 5. Tangential component of the magnetic field across the MP from global MHD simulations (magenta and blue lines), Vlasov equilibrium modeling (in black), and in situ MMS2 observations (in red). The profile MHD sig1 is a spatial profile obtained from a time snapshot of the 3-D global MHD simulation; MHD sig2 considers the time-dependent evolution of global simulations (see Section 3).

sig1 and sig2 and not for the MMS2 signal, which was displaced by 1.8 R_E such that the center of its MP transition would coincide with the center of sig1 and sig2.

The MP profile for plasma density exhibits characteristics similar to the magnetic field transition, as shown in Figure 7 and the enlarged view of its central region provided in Figure 8. We note that the variation in density at the MP had a slightly larger scale compared with the magnetic field, on the order of 10,000 km. The spatial profile taken from a time snapshot (sig2) exhibited a slightly smaller scale, on the order of 8000 km. The MP density gradient resulting from global MHD simulations was much smaller than the one observed in situ by MMS2 and the one provided by the Vlasov model. Note also that the open–closed magnetic field boundary (or MP) location from global MHD simulations is at R_n = +1210 km in Figure 7.

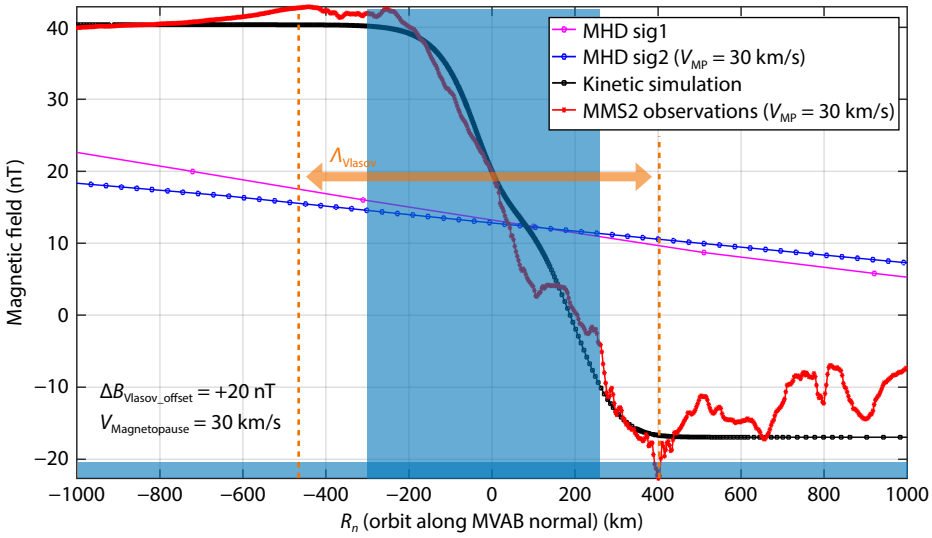

Figure 6. Same as Figure 5 but for the central region of the transition. A magnetic offset between the Vlasov magnetic field and MMS2 on the order of 20 nT was compensated for such that the asymptotic values overlapped.

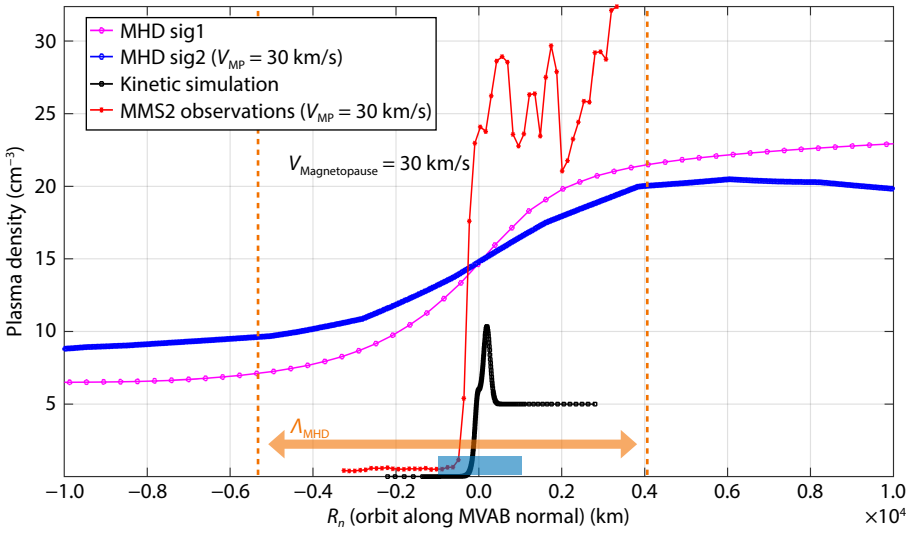

Figure 7. Plasma density at the MP from global MHD simulations (magenta and blue lines), Vlasov equilibrium modeling (in black), and in situ MMS2 observations (in red). The profile MHD sig1 is a spatial profile obtained from a time snapshot of the 3-D global MHD simulation; MHD sig2 considers the time-dependent evolution of global simulations (see discussion in Section 3).

A third parameter that was investigated is the tangential component of the plasma bulk velocity and its variation across the MP, as shown in Figures 9 and 10. The spatial scale for the velocity transition from global MHD simulations increased compared with the density profile and was on the order of 12,000 km, a bit thinner when the time snapshot was considered (sig1) instead of the explicit time dependence (sig2). However, the MMS2 data indicated that the scale of velocity shear at the MP was smaller than the scale of the magnetic field gradient. The current density from global MHD simulations (not shown) was also much smaller than that from MMS2 observations.

The tangential component of the plasma bulk velocity provided by the Vlasov model was in good agreement with MMS2 observations. The spatial scale was on the order of 400 km (compared with 500 km from MMS2 data), and the asymptotic values, both upstream and downstream, took values close to the MMS2 observations. The velocity gradient was also in agreement with the data, as shown in Figure 10.

Thus, a comparison between in situ observations of the MP at the dusk flank and the results of global MHD simulations and Vlasov modeling tailored to the observations showed that generally, the spatial scales and gradients provided by global MHD simulations were one order of magnitude larger than the scales and gradients provided by observations. The Vlasov model provides a good estimation of the scales and gradients, compared with observations. The profile of transition has different spatial scales for different parameters (magnetic field, tangential component of the bulk velocity) derived from the simulations and, to a lesser extent, for the Vlasov model and in situ data.

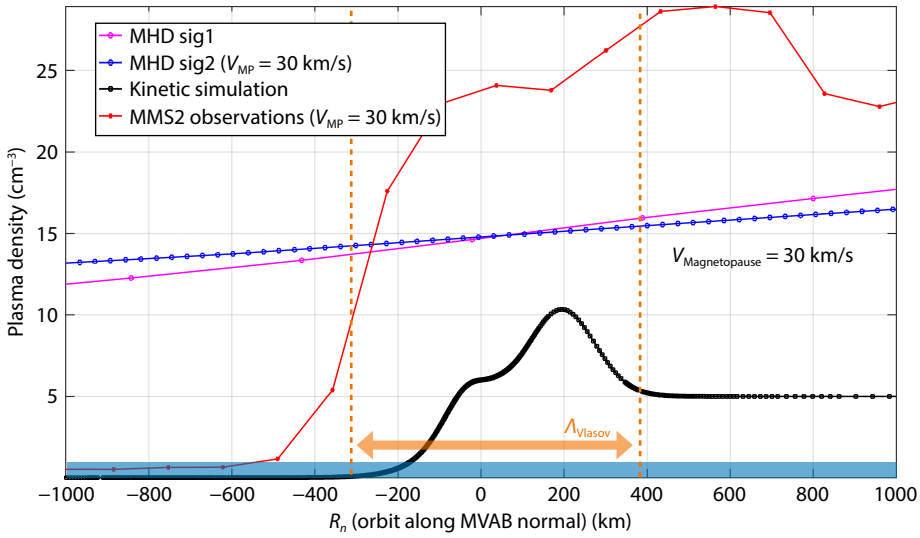

Figure 8. Same as Figure 7 but with an enlarged view of the central MP region. In situ measurements from MMS2 also indicate that the density has a "bump" in the MP transition region, where the density increases by 20%. A similar feature is found in the Vlasov kinetic solution and is due to a population trapped inside the MP, which could be considered to carry the Chapman–Ferraro current. The spatial scale of the density profile in the Vlasov model is on the order of 700 km, in good agreement with the MMS2 data. Nevertheless, even though the asymptotic Vlasov model density downstream of the MP is in agreement with MMS2, the density upstream takes a smaller value in the Vlasov equilibrium than it does in situ.

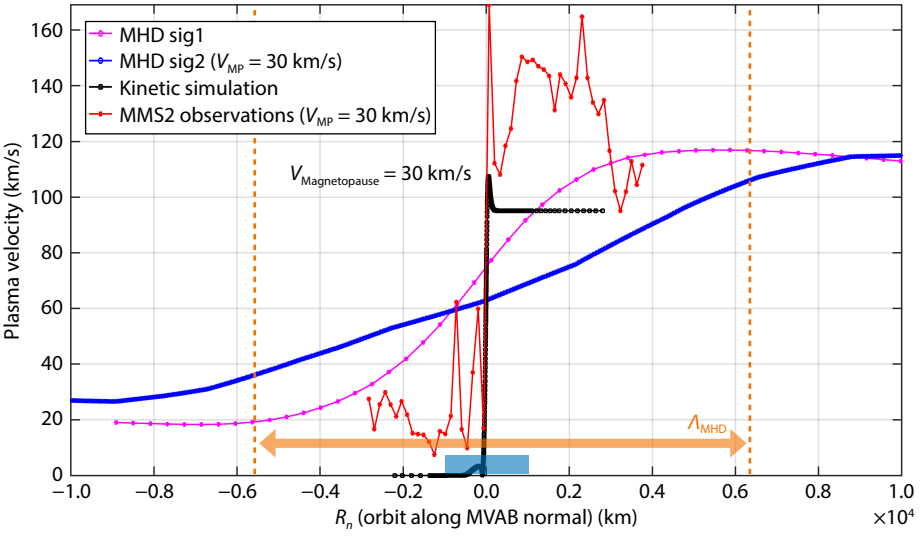

Figure 9. The tangential component of the plasma bulk velocity at the MP from global MHD simulations (magenta and blue lines), Vlasov equilibrium modeling (in black), and in situ MMS2 observations (in red). The profiles MHD sig1 and MHD sig2 were derived as explained in Figure 5 and 7.

5. Summary, Conclusions, and Perspectives

We performed global numerical simulations with the SWMF/GM (BATS-RUS) module on the NASA-CCMC model initialized with solar wind conditions extracted from the OMNI database precisely for the time interval (on October 16, 2015) when the MMS2 spacecraft intersected the dusk side MP (Haaland et al., 2020). We also calculated 1-D profiles for the MP for boundary conditions extracted from in situ observations provided by MMS2 on the respective date. Both the global simulations and the Vlasov model showed similarities and differences compared with the observations, which can be summarized as shown below.

The MP properties derived at the dusk flank from global MHD simulations performed with SWMF/GM (BATS-RUS) code showed the following similarities with in situ measurements by MMS2:

- The tangential component of the magnetic field showed a transition from positive to negative values. The overall magnetic jump was on the order of the observed one.
- The general trend for density showed an increase across the MP.
- The tangential component of the bulk velocity increased from the downstream to upstream MP.

However, we also found significant differences between the MP properties from global numerical simulations and in situ data:

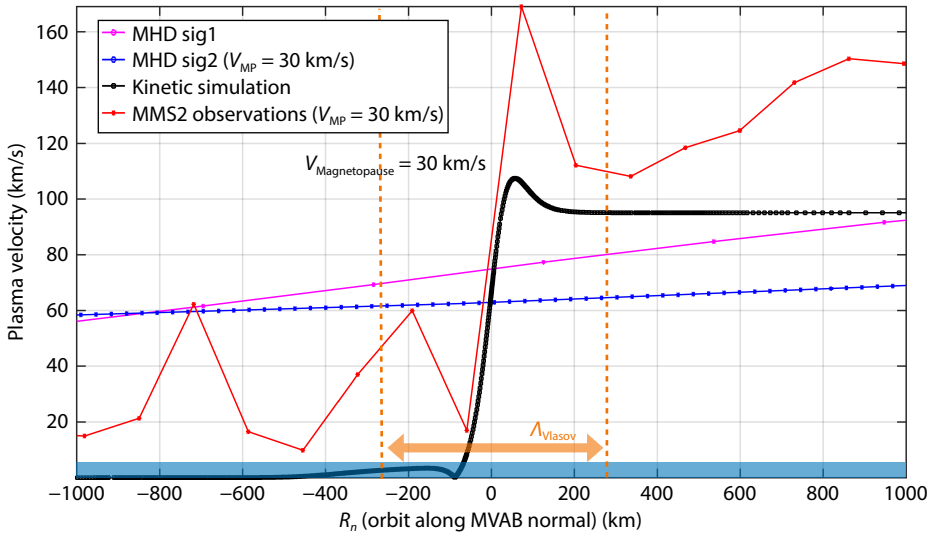

Figure 10. Same as Figure 9 but for an enlarged view of the central MP region.

• The MP was located closer to the Earth by 1.8 R_E compared with the real position observed in the dusk sector by MMS2.
• The spatial scale of the transition for all the parameters considered (tangential magnetic field, density, tangential component of the bulk velocity) was one order of magnitude larger than observed.
• The total jump in density and the tangential component of the bulk velocity was smaller than observed.
• The gradients of all parameters were significantly smaller than observed.

The local, time-independent, 1-D Vlasov equilibrium model derived from asymptotic conditions consistent with MMS2 observations at the MP had the following similarities with observations:
• The Vlasov equilibrium describes a transition with sheared velocities, in good agreement with the observations.
• The Vlasov equilibrium describes a gradient of the plasma density, with a larger density at the right (magnetosheath) side.
• The Vlasov equilibrium describes sheared magnetic fields, with a magnetic reversal of the tangential component and vanishing normal components.
• The spatial scales of the transition for all three parameters considered (tangential component of the magnetic field, bulk velocity, plasma density) were in good agreement with the transition scales observed by MMS2.
• The overall jump in density and the tangential component of the bulk velocity was in agreement with observations.
• Specific features, such as a density bump observed by MMS2 inside the MP, were captured by the Vlasov model.
• The gradients were in agreement with observations.

The Vlasov model also showed some inconsistencies with observations:
• There was a magnetic offset of approximately 20 nT between the Vlasov model and observations.
• The density on the magnetosheath side was underestimated by the Vlasov model.
• The asymptotic bulk velocity also showed some differences.

In summary, the global MHD simulations allowed a good estimation of the asymptotic conditions at the MP, but the position of the MP, the thickness, and the gradients were not consistent with in situ measurements. The kinetic modeling reproduced the thickness and gradients well but introduced a magnetic offset and differences for the asymptotic plasma density compared with observations. In studies devoted to the SMILE mission based on observational scenarios derived from simulated 3-D global magnetospheric dynamics, some of the similarities and differences mentioned might have a significant impact.

The location of the MP in global MHD simulations was determined as the open–closed magnetic field line boundary and was found to be closer to the Earth than in the MMS2 data; this effect might artificially enhance the soft X-ray emissivity at the MP because of an increased value of the exospheric density (Samsonov et al., 2022a). Indeed, the latter decreases with r^{-3}, the radial distance from the center of the Earth. The much smoother gradients at the MP provided by the global MHD simulations coupled with the magnetospheric masking procedure (Samsonov et al., 2022b) might reduce the MP contrast in the synthetic images of the MP provided by the SMILE-SXI simulator, based on global MHD numerical results.

More specifically, when the magnetospheric masking is applied (e.g., see Samsonov et al., 2022a,b), the MP is treated as a sharp or infinitesimal jump from density values provided by the global MHD simulations in the magnetosheath, upstream of the modeled MP, to a density equal to zero downstream of the MP, in the magnetosphere. We believe it is feasible, in a continuation of this study, to test approaches that can combine the global MP picture revealed by the global 3-D MHD numerical simulations with the local 1-D Vlasov description of the MP. One can attempt to replace the sharp MP jump assumed by the masking procedure with a smoother profile provided by kinetic modeling. Although such a combined image of the MP (from global MHD and kinetic modeling) will not be self-consistent, it will, however, provide an observational scenario or "scene" bearing more realistic properties of the MP (in terms of thickness and gradients), thus allowing further testing of the observational performance in preparation for SMILE SXI imaging of the MP.

Acknowledgments

The authors acknowledge support from the European Space Agency (ESA) PRODEX (PROgramme de Développement d'Expériences scientifiques) Project mission (No. PEA4000134960). Partial funding was provided by the Romanian Ministry of Research, Innovation and Digitalization under Romanian National Core Program LAPLAS VII (Contract No. 30N/2023) and the Belgian Solar-Terrestrial Centre of Excellence. M.E. is supported by the project Belgian Research Action through Interdisciplinary Networks (BRAIN-BE) 2.0 (Grant No. B2/223/P1/PLATINUM) funded by the Belgian Office for Research (BELSPO). This work was partially supported by a grant from the Romanian Ministry of Education and Research (CNCS-UEFISCDI, Project No. PN-III-P1-1.1-TE-2021-0102). The global simulation results used in this study are publicly available from the NASA-CCMC: https://ccmc.gsfc.nasa.gov/results/viewrun.php?domain=GM&runnumber=Gabriel_Voitcu_100421_1. The MMS2 data are publicly available through https://lasp.colorado.edu/mms/sdc/public/. The MMS MP crossing database is hosted by the International Space Science Institute in Bern (Paschmann et al., 2018; Haaland et al., 2020); access is granted by request. The Vlasov equilibrium solutions discussed in this study are available from the public repository hosted by the Royal Belgian Institute for Space Aeronomy.

References

Branduardi-Raymont, G., and Wang, C. (2022). The SMILE mission. arXiv: 2208.03757. https://doi.org/10.48550/arXiv.2208.03757

Burlaga, L. F., and Lemaire, J. F. (1978). Interplanetary magnetic holes: Theory. *J. Geophys. Res.: Space Phys.*, *83*(A11), 5157–5160. https://doi.org/10.1029/JA083iA11p05157

Cahill, L. J., and Amazeen, P. G. (1963). The boundary of the geomagnetic field. *J. Geophys. Res.*, *68*(7), 1835–1843. https://doi.org/10.1029/JZ068i007p01835

Chapman, S., and Ferraro, V. C. A. (1930). A new theory of magnetic storms. *Nature*, *126*(3169), 129–130. https://doi.org/10.1038/126129a0

De Keyser, J., and Roth, M. (1997). Equilibrium conditions for the tangential discontinuity magnetopause. *J. Geophys. Res.: Space Phys.*, *102*(A5), 9513–9530. https://doi.org/10.1029/97JA00335

De Keyser, J., and Roth, M. (1998). Equilibrium conditions and magnetic field rotation at the tangential discontinuity magnetopause. *J. Geophys. Res.: Space Phys.*, *103*(A4), 6653–6662. https://doi.org/10.1029/97JA03710

Delcroix, J. L., and Bers, A. (1994). *Physique Des Plasmas*. Les Ulis: EDP Sciences.

Echim, M., Maggiolo, R., De Keyser, J., Zhang, T. L., Voitcu, G., Barabash, S., and Lundin, R. (2011). Comparative investigation of the terrestrial and Venusian magnetopause: Kinetic modeling and experimental observations by Cluster and Venus Express. *Planet. Space Sci.*, *59*(10), 1028–1038. https://doi.org/10.1016/j.pss.2010.04.019

Echim, M. M., and Lemaire, J. F. (2005). Two-dimensional Vlasov solution for a collisionless plasma jet across transverse magnetic field lines with a sheared bulk velocity. *Phys. Rev. E*, *72*(3), 036405. https://doi.org/10.1103/PhysRevE.72.036405

Escoubet, P., Russell, C., Schmidt, R. (1997). The Cluster and PHOENIX missions. Dordrecht: Kluwer.

Glocer, A., Tóth, G., Ma, Y., Gombosi, T., Zhang, J. C., and Kistler, L. M. (2009). Multifluid Block-Adaptive-Tree Solar wind Roe-type Upwind Scheme: Magnetospheric composition and dynamics during geomagnetic storms—Initial results. *J. Geophys. Res.: Space Phys.*, *114*(A12), A12203. https://doi.org/10.1029/2009JA014418

Gombosi, T. I., Tóth, G., De Zeeuw, D. L., Hansen, K. C., Kabin, K., and Powell, K. G. (2002). Semirelativistic magnetohydrodynamics and physics-based convergence acceleration. *J. Comput. Phys.*, *177*(1), 176–205. https://doi.org/10.1006/jcph.2002.7009

Gurnett, D. A., and Bhattacharjee, A. (2017). *Introduction to Plasma Physics* (2nd ed.). Cambridge: Cambridge University Press. https://doi.org/10.1017/9781139226059

Haaland, S., and Gjerloev, J. (2013). On the relation between asymmetries in the ring current and magnetopause current. *J. Geophys. Res.: Space Phys.*, *118*(12), 7593–7604. https://doi.org/10.1002/2013JA019345

Haaland, S., Paschmann, G., Øieroset, M., Phan, T., Hasegawa, H., Fuselier, S. A., Constantinescu, V., Eriksson, S., Trattner, K. J., … Burch, J. (2020). Characteristics of the flank magnetopause: MMS results. *J. Geophys. Res.: Space Phys.*, *125*(3), e2019JA027623. https://doi.org/10.1029/2019JA027623

Haaland, S., Hasegawa, H., Paschmann, G., Sonnerup, B., and Dunlop, M. (2021). 20 years of Cluster observations: The magnetopause. *J. Geophys. Res.: Space Phys.*, *126*(8), e2021JA029362. https://doi.org/10.1029/2021JA029362

Hudson, P. D. (1970). Discontinuities in an anisotropic plasma and their identification in the solar wind. *Planet. Space Sci.*, *18*(11), 1611–1622. https://doi.org/10.1016/0032-0633(70)90036-X

Khrabrov, A. V., and Sonnerup, B. U. Ö. (1998). Orientation and motion of current layers: Minimization of the Faraday residue. *Geophys. Res. Lett.*, *25*(13), 2373–2376. https://doi.org/10.1029/98GL51784

Lemaire, J., and Burlaga, L. F. (1976). Diamagnetic boundary layers: A kinetic theory. *Astrophys. Space Sci.*, *45*(2), 303–325. https://doi.org/10.1007/BF00642667

Mailyan, B., Munteanu, C., Haaland, S. (2008). What is the best method to calculate the solar wind propagation delay?. *Annales Geophysicae*, 26(8), 2383–2394. https://doi.org/10.5194/angeo-26-2383-2008

Montgomery, D. C., and Tidman, D. A. (1964). *Plasma Kinetic Theory*. New York: McGraw-Hill.

Munteanu, C., Haaland, S., Mailyan, B., Echim, M., and Mursula, K. (2013). Propagation delay of solar wind discontinuities: Comparing different methods and evaluating the effect of wavelet denoising. *J. Geophys. Res.: Space Phys.*, *118*(7), 3985–3994. https://doi.org/10.1002/jgra.50429

Paschmann, G., Haaland, S. E., Phan, T. D., Sonnerup, B. U. Ö., Burch, J. L., Torbert, R. B., Gershman, D. J., Dorelli, J. C., Giles, B. L., … Fuselier, S. A. (2018). Large-scale survey of the structure of the dayside magnetopause by MMS. *J. Geophys. Res.: Space Phys.*, *123*(3), 2018–2033. https://doi.org/10.1002/2017JA025121

Raab, W., Branduardi-Raymont, G., Wang, C., Dai, L., Donovan, E., Enno, G., Escoubet, P., Holland, A., Jing, L., … Zheng, J. H. (2016). SMILE: A joint ESA/CAS mission to investigate the interaction between the solar wind and Earth's magnetosphere. In *Proceedings Volume 9905, Space Telescopes and Instrumentation 2016: Ultraviolet to Gamma Ray*. Edinburgh, United Kingdom: SPIE. https://doi.org/10.1117/12.2231984

Roth, M. (1978). Structure of tangential discontinuities at the magnetopause: The nose of the magnetopause. *J. Atmos. Terr. Phys.*, *40*(3), 323–329. https://doi.org/10.1016/0021-9169(78)90048-X

Roth, M., De Keyser, J., and Kuznetsova, M. M. (1996). Vlasov theory of the equilibrium structure of tangential discontinuities in space plasmas. *Space Sci. Rev.*, *76*(3-4), 251–317. https://doi.org/10.1007/BF00197842

Samsonov, A., Carter, J. A., Read, A., Sembay, S., Branduardi-Raymont, G., Sibeck, D., and Escoubet, P. (2022a). Finding magnetopause standoff distance using a soft X-ray imager: 1. Magnetospheric masking. *J. Geophys. Res.: Space Phys.*, *127*(12), e2022JA030848. https://doi.org/10.1029/2022JA030848

Samsonov, A., Sembay, S., Read, A., Carter, J. A., Branduardi-Raymont, G., Sibeck, D., and Escoubet, P. (2022b). Finding magnetopause standoff distance using a soft X-ray imager: 2. Methods to analyze 2-D X-ray images. *J. Geophys. Res.: Space Phys.*, *127*(12), e2022JA030850. https://doi.org/10.1029/2022JA030850

Sestero, A. (1964). Structure of plasma sheaths. *Phys. Fluids*, *7*(1), 44–51. https://doi.org/10.1063/1.1711053

Sestero, A. (1966). Vlasov equation study of plasma motion across magnetic fields. *Phys. Fluids*, *9*(10), 2006–2013. https://doi.org/10.1063/1.1761559

Sestero, A. (1967). Self-consistent description of a warm stationary plasma in a uniformly sheared magnetic field. *Phys. Fluids*, *10*(1), 193–197. https://doi.org/10.1063/1.1761973

Soman, M. R., Hall, D. J., Holland, A. D., Burgon, R., Buggey, T., Skottfelt, J., Sembay, S., Drumm, P., Thornhill, J., … Woffinden, C. (2018). The SMILE Soft X-ray Imager (SXI) CCD design and development. *J. Inst.*, *13*(1), C01022. https://doi.org/10.1088/1748-0221/13/01/C01022

Sonnerup, B.U.O., Scheible, M. (1998). Minimum and maximum variance analysis. In: Götz Paschmann and Patrick Daly eds. Analysis Methods for Multi-Spacecraft Data. ISSI Scientific Reports Series, ESA/ISSI, Vol. 1. ISBN 1608-280X, p. 185–220.

Tóth, G., De Zeeuw, D. L., Gombosi, T. I., and Powell, K. G. (2006). A parallel explicit/implicit time stepping scheme on block-adaptive grids. *J. Comput. Phys.*, *217*(2), 722–758. https://doi.org/10.1016/j.jcp.2006.01.029

Tóth, G., Ma, Y. J., and Gombosi, T. I. (2008). Hall magnetohydrodynamics on block-adaptive grids. *J. Comput. Phys.*, *227*(14), 6967–6984. https://doi.org/10.1016/j.jcp.2008.04.010

Whipple, E. C., Hill, J. R., and Nichols, J. D. (1984). Magnetopause structure and the question of particle accessibility. *J. Geophys. Res.*: *Space Phys.*, *89*(A3), 1508–1516. https://doi.org/10.1029/JA089iA03p01508